Single Crystals of V-Amylose Complexed with α-Naphthol

Mateus B. Cardoso,[†,‡] Jean-Luc Putaux,[*,†] Yoshiharu Nishiyama,[†] William Helbert,[†,§] Martin Hÿtch,[#] Nádya P. Silveira,[‡] and Henri Chanzy[†]

Centre de Recherches sur les Macromolécules Végétales (CERMAV-CNRS), BP 53, F-38041 Grenoble Cédex 9, France—affiliated with Université Joseph Fourier and member of the Institut de Chimie Moléculaire de Grenoble, Instituto de Química, Universidade Federal do Rio Grande do Sul, Caixa Postal 15003, CEP 91501-970 Porto Alegre RS, Brazil, and Centre d'Elaboration de Matériaux et d'Etudes Structurales (CEMES-CNRS), 29 Rue Jeanne Marvig, F-31055 Toulouse, France

Received November 25, 2006; Revised Manuscript Received January 26, 2007

Lamellar square single crystals of V-amylose were obtained by adding α-naphthol to metastable dilute aqueous solutions of synthetic amylose chains with an average degree of polymerization of 100. The morphology and structure of the crystals were studied using low-dose transmission electron microscopy including high-resolution imaging, as well as electron and X-ray diffraction. The crystals are crystallized in a tetragonal $P4_12_12$ or $P4_32_12$ space group with unit cell parameters, calculated from X-ray diffraction data, $a = b = 2.2844$ nm (±0.0005) and $c = 0.7806$ nm (±0.001), implying the presence of two amylose chains per unit cell. High-resolution lattice images of the crystals confirmed that the amylose chains were crystallized as 8-fold helices corresponding to the repeat of four maltosyl units.

Introduction

In contrast with its molecular simplicity, amylose is extremely versatile in its mode of crystallization. In its native form, this linear (1→4)-α-D-glucan essentially crystallizes in the A and B allomorphs, which both consist of the parallel packing of double helices associated with a number of water molecules.[1−4] A-amylose chiefly occurs in cereal starches whereas B-amylose is mainly found in tuber starches. Besides these two allomorphs, which can also be obtained by crystallization from aqueous solutions,[5−7] a number of single helical amylose complexes, categorized under the generic name of V-amylose, have been described.[8] The multiplicity of V-amylose crystals takes its origin in the remarkable number of hydrophobic or hydrophilic inorganic and organic guests that are susceptible to becoming associated with amylose helices serving as hosts.[9,10] The study of these complexes presents a great interest since the guest molecules that have been trapped at some stage can be released later, thus leading to many applications, in particular in pharmacology and in the food industry.

Some of the crystalline V-amylose complexes yield well-resolved X-ray fiber diffraction diagrams. Structural models have been proposed but a number of details remain to be determined.[11−15] In particular, it is not always clear to know whether guest molecules are included within the cavity of helical amylose, in between the helices, or in both locations. When crystallized from dilute solution, depending on the guest molecule, amylose can yield remarkable micrometer-sized lamellar single crystals.[5,16−22] They give sharp electron diffraction diagrams provided that precautions are taken to keep the guest molecules within the crystalline domains during the observation in the vacuum of the transmission electron microscope. With amylose in the V form, chain folding does not seem to be a problem, since similar monolamellar crystals with smooth surface can be obtained with any polymer chain length. This beneficial property must be related to the so-called 'flip' that is susceptible to occur between two adjacent glucosyl moieties connected by a (1→4)-α-type of linkage.[23−25] Indeed, this flip, when it occurs, leads to a reversal of the molecular trajectory, thus favoring a chain folding mechanism to form lamellar crystals.

At present, five families of lamellar single crystals of V-amylose have been characterized in terms of morphology and electron diffraction diagrams. Hexagonal crystals of V_H-amylose, exhibiting hexagonal diffractograms, are prepared from the addition of either hot ethanol or fatty acids to aqueous solutions of amylose.[15,18−20] There are two families of rectangular V-amylose crystals presenting two different types of rectangular diffractograms. One of them, under the generic name of $V_{isopropanol}$, corresponds to crystals incorporating either isopropanol or a wealth of other complexing agents, namely some alcohols, ketones, as well as a number of organic reagents.[22,26,27] $V_{butanol}$ crystals, which result from the addition of *n*-butanol or *n*-pentanol, correspond to the other family.[17,18,21,28,29] Square $V_{glycerol}$ crystals, diffracting along a nearly 4-fold symmetry, are formed during the high-temperature crystallization of amylose with glycerol in the absence of water.[30] A fifth family is obtained with α-naphthol or quinoline as complexing agents. The crystals of $V_{\alpha-naphthol}$ have a squarish shape and yield electron diffractograms with 4-fold symmetry.[31−33] It is likely that the number of families of lamellar single crystals of V-amylose will be greater than 5. Among the candidates, it seems that V_a or V_{DMSO} amylose should also yield lamellar single crystals, since both allomorphs can be readily crystallized to a substantial perfection, denoted by well-resolved X-ray diagrams.[12,34,35] However, so far, all our attempts of crystallizing these allomorphs from dilute solutions have resulted in the production of shapeless precipitates but not lamellae.

* Corresponding author. E-mail: putaux@cermav.cnrs.fr. Fax: +33 476 54 72 03.

† CERMAV-CNRS.

‡ Universidade Federal do Rio Grande do Sul.

§ Present address: Végétaux Marins et Biomolécules, UMR 7139 (CNRS-Université Pierre et Marie Curie, Paris VI), Station Biologique, BP 74, F-29682 Roscoff, France.

CEMES-CNRS.

10.1021/bm0611174 CCC: $37.00
Published on Web 03/10/2007

The resolution of the crystal structure of V_H-amylose has shown that this allomorph consisted of the hexagonal close packing of left-handed 6-fold amylose helices, together with intra- and extrahelical molecules of water.[11,13,15] In the V_H case, the intrahelical cavity may also accept a number of linear guests,[25,36−37] but there is no room for them in between the helices. Upon selective drying, the crystals of $V_{butanol}$, $V_{isopropanol}$, and $V_{glycerol}$ invariably yield V_H electron diffraction diagrams,[17,21,22,29,30] which suggests that these crystalline complexes also consist of left-handed 6-fold amylose helices, with some of the guest molecules located between the helices. The $V_{isopropanol}$ crystals have also been described as made of 7-fold helices by analogy with β-cyclodextrins.[26] However, their reversible conversion into the 6-fold V_H structure without change in morphology is questioning the occurrence of 7-fold helices in these crystals.

The case of the $V_{\alpha-naphthol}$ crystals is drastically different from that of 6-fold V-amylose since, in this complex, the amylose chains are thought to form 8-fold helices.[31−33] At present, almost no firm data exists on this type of V-amylose complexes. The only crystals described so far have rather poor shapes, and nothing is known regarding their stability. In our continuous interest in unraveling the crystalline properties of amylose, we have undertaken the preparation and analysis of crystals of $V_{\alpha-naphthol}$ single crystals with the goal of solving their molecular structure. The present paper describes the preparation of these lamellar crystals and their description using X-ray diffraction analysis together with electron crystallography techniques, involving three-dimensional electron diffraction analysis and high-resolution electron microscopy (HREM) imaging. Subsequent reports will show how these data can be used to solve the molecular structure of this complex.

Experimental Section

Preparation of the Crystals. Synthetic amylose with an average degree of polymerization (DP) of 100, a gift from Dr. Gessler (Free University of Berlin, Germany), was dispersed in water (0.05% w/v), and α-naphthol was added in a proportion of 1:3 (w/w) with respect to the amylose. The mixture was submitted to nitrogen bubbling for 20 min and then sealed in a vial, which was heated to 150 °C by immersion in an oil bath. After 60 min, the solution was filtered through a 0.2 μm preheated filter, and the filtrate was kept at 95 °C for 2 h before being cooled to room temperature. Crystallization occurred overnight.

Density Measurement. A film resulting from the drying of a $V_{\alpha-naphthol}$ crystal suspension was floated on chloroform to which cyclohexane was slowly added. The density of the mixture was measured when the film sank to remain in equilibrium in the mixture of liquids.

Transmission Electron Microscopy and Electron Diffraction. Drops of crystal suspensions were deposited on glow-discharged carbon-coated grids and allowed to dry. For the recording of electron diffraction, some specimens were observed at room temperature and mounted on a Philips rotation holder whereas others were mounted on a Gatan 626 cryo-holder operated at liquid nitrogen temperature. In this latter case, the specimens were quench-frozen in liquid nitrogen prior to insertion in the electron microscope in order to prevent any evaporation of the α-naphthol in the vacuum of the microscope. Base plane electron diffraction diagrams corresponding to *hk*0 reflections were collected either at room or liquid nitrogen temperature on crystals with lamellar base perpendicular to the electron beam. Diagrams containing upper layer line reflections were recorded on crystals that were tilted around selected reciprocal axes. Electron diffraction diagrams were recorded on 1 μm^2 circular areas of single crystals. For calibration purpose, crystals were deposited onto carbon and gold-coated TEM grids, and the diffraction spots were calibrated at room temperature using the diffraction rings of gold as standards. The beam sensitivity of the electron diffraction diagrams was measured by recording sequential diffraction patterns on the same area of one crystal and observing the disappearance of the diffraction spots.[38] In these experiments, the intensity of the impinging beam was measured with a Faraday cup, which also helped to calibrate the response of the microscope fluorescent screen.

All observations were performed with a Philips CM200 'Cryo' electron microscope operated at 80 kV for conventional imaging and 200 kV for electron diffraction and high-resolution imaging. Images were recorded on Kodak SO163 films and diffraction patterns on Fujifilm imaging plates, read with a Fujifilm BAS-1800II bioimaging analyzer.

High-Resolution Electron Microscopy. HREM imaging was performed at room temperature with the specimen mounted in a simple-tilt holder. Images were recorded on Kodak SO163 films, at magnifications of 38 000× and 50 000×. No objective aperture was used. Prior to image recording, the crystals were selected by searching the specimen in diffraction mode, with a very low illumination. When the diffraction pattern exhibited high symmetry and spot intensity, the beam was immediately blanked, the microscope switched into imaging mode, and the illumination increased. The beam was deblanked and the plate exposed for 1−2 s corresponding to underexposures of a factor 8 with respect to the automatic exposure time. Laser diffractometry on an optical bench was used to select diffracting areas in the HREM negatives. The regions of interest were chosen depending on the symmetry and resolution of the observed spot pattern. The selected areas were photographically enlarged 4 times on Kodak 4489 films and digitized using an 8 bits Kodak Megaplus digital CCD camera. The images were processed on a Silicon Graphics workstation using the Semper 6.4 program (Synoptics, U.K.).[39]

Synchrotron X-ray Diffraction. Synchrotron X-ray experiments were performed on the BM1 beamline at the European Synchrotron Radiation Facility (ESRF, Grenoble, France), using a 0.2 × 0.2 mm^2 monochromatic beam (λ = 0.07840 nm). A suspension of $V_{\alpha-naphthol}$ crystals was allowed to evaporate in flat polyethylene capsules. Pieces of the resulting mats were introduced in 1.0 mm o.d. glass capillaries and mounted on a 3-axis goniometer. A series of textured diagrams were recorded by changing the orientation of the mat with respect to the incident beam. The diffraction diagrams were collected using a MAR345 imaging plate recorder, positioned about 165 mm from the sample, and scanned with a 100 μm resolution. A powder diffraction pattern of LaB_6 was collected under the same conditions to calibrate the detector distance, the detector tilt, and the position of the center. The sample tilts and rotations were measured from the azimuthal angles of *hk*0 reflections. Using these values, the diffraction diagrams were mapped into reciprocal space, and the background subtracted using a Sonneveld and Visser algorithm extended in two dimensions.[40,41] The position of low-resolution X-ray diffraction peaks was measured by fitting Gaussian functions and a linear baseline to the radial line profile. The unit cell parameters were determined from the positions of the 200 and 111 peaks that are strong and not influenced by neighboring reflections. The position of these peaks was determined by least-square fitting of the radial profiles.

Results

Figure 1 shows typical $V_{\alpha-naphthol}$ lamellar crystals. They have a more or less square shape, with a lateral size ranging from 0.5 to 2 μm, and appear to be made of several superimposed square unilamellar crystals. Smaller spherical particles are also observed and are thought to correspond to α-naphthol in excess. Sometimes, such particles are seen embedded in the lamellar crystals, which suggests that they may act as nucleating agents for the crystallization of amylose chains.

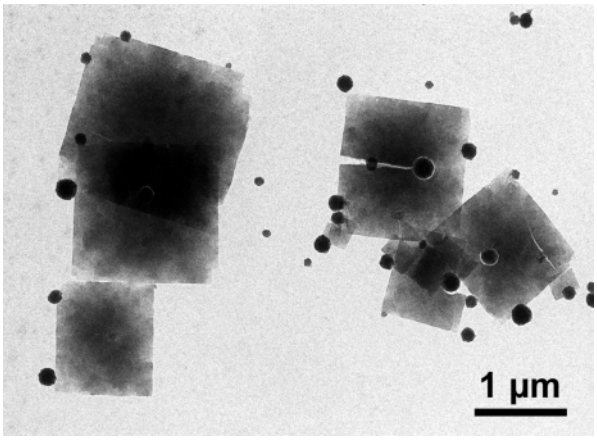

Figure 1. Lamellar single crystals of V-amylose complexed with α-naphthol. Dark spherical particles likely correspond to α-naphthol in excess.

The $V_{\alpha-naphthol}$ crystals had good stability in vacuum, i.e., they did not exhibit any important decomplexation phenomenon. The crystals also demonstrated a substantial stability toward the electron beam. A plot of the intensity of the main diffraction spots against the dose received indicated that the dose at half-life of the diffraction diagram was about 600 e^-/nm^2, at 200 kV and at room temperature. The value of this half-life dose is twice as large as the one observed for other crystalline polysaccharides such as highly crystalline cellulose.[42]

A typical electron diffraction pattern recorded on an untilted $V_{\alpha-naphthol}$ single crystal (Figure 2A) at low temperature is presented in Figure 2B. It contains about 560 spots organized along two orthogonal axes with reciprocal base vectors a^* and b^* of equal length. The diagram extends up to a resolution of about 0.13 nm and displays four symmetry axes: two along a^* and b^* and two at 45° with respect to a^* and b^*. This diagram has thus the 4*mm* symmetry, and since only the reflections indexed with $h0$ or $0k = 2n$ are present along a^* and b^* axes (Figure 2C), it belongs to the two-dimensional *p*4*g* square space group. When accounting for these symmetry elements, the diagram consists of 8 equivalent sectors and thus it contains an overall number of 80 independent reflections.

The symmetry of the three-dimensional structure was obtained by rotating $V_{\alpha-naphthol}$ crystals about selected reciprocal axes. It was found that the patterns recorded by tilting the crystals by a given angle around axes a^* and b^* were identical. Axes a^* and b^* are thus crystallographically equivalent. Moreover, the diffraction diagrams recorded by tilting the crystals clockwise around axes a^* or b^* were identical to those from crystals tilted anticlockwise by the same angle. This equivalence indicates that the c^* axis is perpendicular to the (a^*, b^*) plane and, therefore, that the three-dimensional space group of the $V_{\alpha-naphthol}$ complex is tetragonal.

A sampling of the patterns corresponding to diffraction zones accessible within the limits of our microscope goniometer is presented in Figure 3. Figure 3A shows patterns obtained by tilting the crystals by ±26° and ±36° around the a^* axis and corresponding to the $[01\bar{6}]$ and $[01\bar{4}]$ zones, respectively. Diagrams corresponding to $[01\bar{5}]$ (±30°) and $[01\bar{3}]$ (±44°) zones were also recorded but are not presented here. By tilting the crystals by ±40° and ±47° around the axis defined by $a^* + b^*$, patterns corresponding to the $[1\bar{1}5]$ and $[1\bar{1}4]$ zones, respectively, were recorded (Figure 3B). A diagram corresponding to the $[1\bar{1}6]$ zone (±35°) was also recorded but is not shown here.

The list of observed electron diffraction spots, together with indexation and corresponding *d*-spacings to a resolution of 0.15 nm, is presented in Table 1, available as Supporting Information. The unit cell parameters were calculated using a least-square refinement program from a data set recorded at room temperature. We found the following: $a = b = 2.326$ nm (±0.001) and c (chain axis) = 0.788 nm (±0.001), in agreement with previous results.[31−33] A density of 1.48 g/cm^3 was measured experimentally on a film consisting of a mat of single crystals. In line with the 8-fold amylose structure helix proposed by Yamashita and Monobe,[31] this unit cell could accommodate two amylose helices consisting of 16 glucosyl residues and 8.5 molecules of α-naphthol, assuming that there is no water molecules in the structure. In this scheme, each amylose helix should be positioned on a 4-fold screw axis, with the implication that the independent repeat unit would not be a glucosyl but a maltosyl residue. Since in the diagram shown in Figure 2C only the reflections with indices $h00$ and $0k0 = 2n$ are present along a^* and b^* axes, the likely space group is either $P4_12_12$ (with amylose forming a right-handed helix) or $P4_32_12$ (with a left-handed helix). Both space groups imply that the helices are arranged in an antiparallel fashion.

Figure 4A represents an X-ray diffraction diagram recorded on a mat of sedimented crystals, recorded with the X-ray beam inclined by 11° with respect to the mat surface. This angle was chosen in order to bring the 004 reflection into Bragg condition. The diagram in Figure 4A corresponds to a fiber diagram, consisting of a number of arcs, each of them having an angular spread (full width at half-maximum) of about 35°. This arcing reflects the misalignment of the individual lamellae within the mat, a phenomenon that likely results from uneven deposition of the lamellae during their sedimentation and subsequent drying. The radial broadening of the peaks was very small and corresponded approximately to the size of the incident beam (Figure 4B). No $00l$ reflection was observed up to 0.1 nm resolution. The 004 reflection, which is allowed in both $P4_12_12$ and $P4_32_12$ space groups, was not observed. It is probably very weak or even absent due to the overall 8-fold symmetry of the helix, which brings the intensity of the 004 reflection to a minimum. The 008 reflection, which should be present, is too far out in reciprocal space to be recorded with our equipment. A list of the observed X-ray diffraction spots, together with indexation and corresponding *d*-spacing is presented in Table 2, available as Supporting Information. The unit cell parameters deduced from the X-ray diffraction patterns are $a = b = 2.2844$ nm (±0.0005) and c = 0.7806 nm (±0.001). As generally observed when comparing data from electron and X-ray diffraction diagrams, the parameters deduced from X-ray diffraction are slightly smaller than those resulting from the analysis of electron diffraction patterns. In other crystalline polysaccharides such as cellulose, such parameter increase under electron irradiation has been attributed to a crystalline swelling resulting from beam damage.[43]

Patterns such as that shown in Figure 4A, which are similar to those recorded by Yamashita and Monobe[31] and Helbert,[33] confirm that the amylose helices are perpendicular to the crystal lamellar planes. Quite remarkably, the value of the c parameter is equivalent, within experimental error, to fiber repeat values determined by diffraction analysis for the V_H,[15] $V_{isopropanol}$,[22] $V_{butanol}$[29] and $V_{glycerol}$[30] complexes.

Figure 5A shows a HREM image of a $V_{\alpha-naphthol}$ crystal recorded at room temperature. Lattice fringes can be seen, although the signal-to-noise ratio is very low and no clear repeating motif can be recognized. The power spectrum (squared

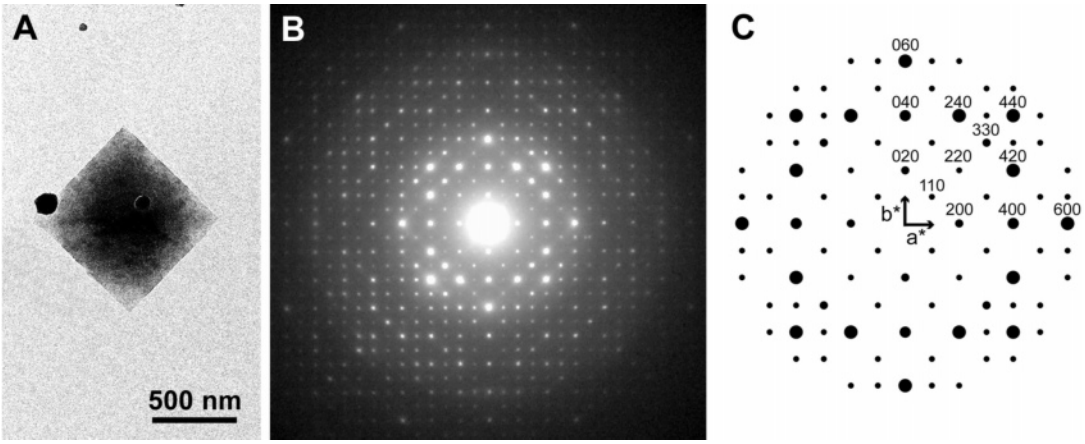

Figure 2. (A) $V_{\alpha-naphthol}$ single-crystal (B) corresponding base plane electron diffraction pattern correctly oriented with respect to the crystal in A; (C) indexation of the pattern in B, up to a resolution of about 0.37 nm. For clarity, only selected reflections have been indexed.

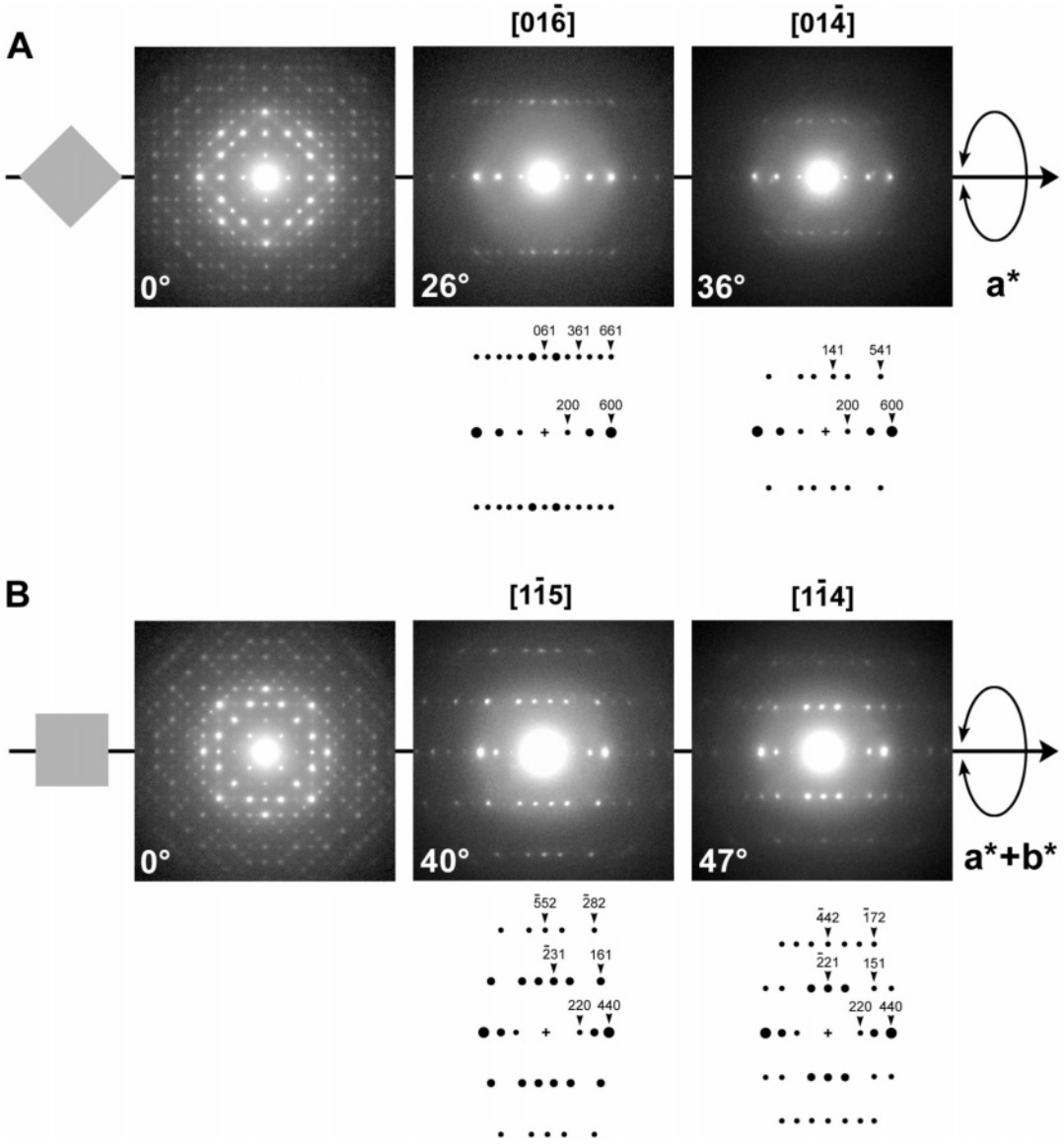

Figure 3. (A) Electron diffraction patterns recorded on $V_{\alpha-naphthol}$ crystals rotated by ±26° and ±36° around *a**; (B) diffraction diagrams recorded on crystals rotated by ±40° and ±47° around *a** + *b**. At the left of both figures, the orientation of the square crystal at 0° tilt angle is schematized in gray. The indexations of selected reflections are shown below the tilted patterns.

Fourier transform of the image) shown in Figure 5B confirms that periodic signals are present in the image. The diagram displays 32 clearly visible diffraction spots mirrored in eight equivalent sectors. It contains seven independent diffraction spots, distributed along six layer lines. This optical diffractogram is identical to the electron diffraction pattern (Figure 2B) up to the 600 and 060 spots, indicating that the HREM image contains crystal information to a 0.388 nm resolution.

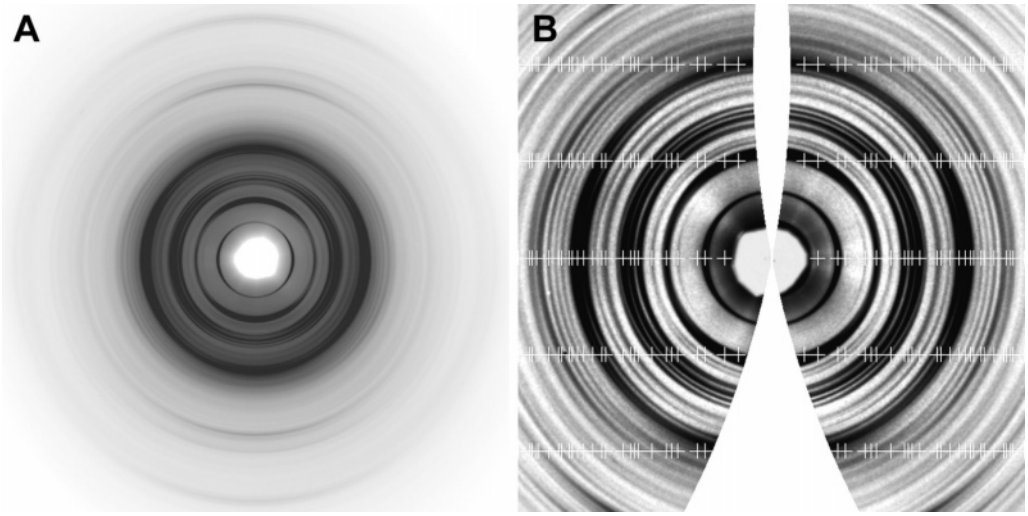

Figure 4. (A) Synchrotron X-ray diffraction fiber diagrams recorded on mats of sedimented $V_{\alpha-naphthol}$ crystals. The X-ray beam is inclined by 11° with respect to the mat plane. (B) Display of the X-ray diffraction pattern after background subtraction using the Sonneveld and Visser algorithm and remapping into cylindrical reciprocal space, up to a resolution of about 0.3 nm. The white crosses correspond to the individual diffraction spots.

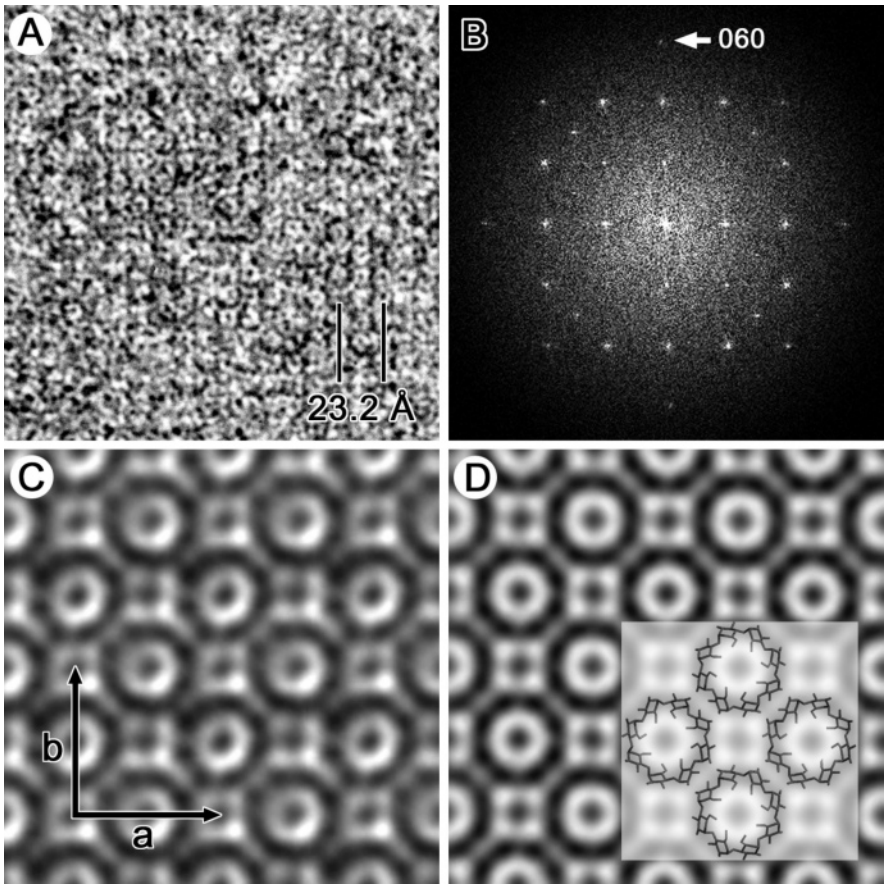

Figure 5. (A) HREM image of a $V_{\alpha-naphthol}$ crystal viewed along the chain axis *c*; (B) power spectrum of the lattice image; (C) real-space translational average; (D) 4-fold rotation average of the image in C. Inset: a molecular model corresponding to the projection of 8-fold amylose helices viewed end-on is superimposed on the average image.

1024 × 1024 pixels^2 images were cut from the original micrograph, with edges parallel to *a* and *b* axes and dimensions corresponding to 32 × 32 $V_{\alpha-naphthol}$ unit cells. Only those that produced power spectra with good symmetry and resolution were kept and submitted to a real-space averaging procedure.[44] First, the positions of reflections 600 and 060 were determined from the optical diffractogram. Then, the reciprocal base vectors a^* and b^*, corresponding to absent reflections 100 and 010, respectively, were deduced, as well as real-space lattice vectors *a* and *b*. The experimental image was cut into elementary square boxes with dimensions corresponding to one unit cell, centered on the nodes of a lattice defined by *a* and *b*. Then, all the boxes were added and an average motif was obtained with a substantially higher signal-to-noise ratio. An average image, built by translating the average motif along *a* and *b*, is shown in Figure 5C. Considering the 4-fold symmetry of the power spectrum (Figure 5B), an additional 4-fold rotational average was calculated from the image in Figure 5C. The result is shown

in Figure 5D and can be described as a square lattice of rings consisting of eight black oval dots.

The knowledge of the phase contrast transfer function (PCTF) is important in order to verify the correspondence between the average image and the projection of the atomic potential in the crystal.[45] The PCTF is generally determined by recording an image of the amorphous supporting carbon film and by analyzing in the calculated diffractogram the so-called Thon rings whose distribution is directly related to the image defocus.[46] In our case, as shown in Figure 5B, we could not measure the image defocus with precision as we could not detect any clear Thon ring. This absence may be due to the fact that the image was recorded with a very low electron dose, resulting in a very poor contrast. In addition, the image may have been recorded at a defocus where the PCTF has a large bandwidth, and therefore extinction rings would not be seen in the diffractogram. If this assumption is correct, the image has thus been recorded with a defocus close to the so-called Scherzer value, where the contrast is maximum and the atoms are seen as black objects. As a consequence, the rings consisting of eight black oval dots in Figure 5D would represent the projection of 8-fold amylose helices along direction *c*, each dot corresponding to a column of glycosyl units. In addition, assuming that the 8-fold amylose helices are in close contact along the diagonal of the unit cell, we can estimate an external helical diameter of 1.62 nm (Figure 5D) which is consistent with the models proposed by Yamashita and Monobe[31] and Winter et al.[32]

Black domains also are seen at the center of the helices and in between. Still assuming that the atoms are seen as black objects, these electron-dense regions may correspond to columns of α-naphthol molecules entrapped in the crystal structure, both inside the helical cavity and in the interstitial space between helices.

Discussion

Among all the V-amylose crystals that have been prepared and investigated in our laboratory, the $V_{\alpha-naphthol}$ single crystals stand out as being by far the most perfect in terms of crystalline organization. Indeed, when they are observed at liquid nitrogen temperature, these crystals yield highly resolved electron diffraction diagrams, extending to a resolution of around 0.1 nm, which is quite unusual for other types of V-amylose crystals as well as other polysaccharides or even synthetic polymers. To our knowledge, such a resolution for polysaccharide crystals was only obtained with a few native fibrous crystals such as those of algal[47] or animal[48] cellulose or chitin specimens such as in *Sagitta*'s grasping spines.[49] Concomitant with this perfection, the $V_{\alpha-naphthol}$ crystals are also quite stable when irradiated with an electron beam. This stability is reflected in the recording of high-resolution images such as that shown in Figure 5A, although it was recorded at room temperature. The lattice is readily revealed, thus indicating that the periodical information of the projected crystalline structure has been preserved to a resolution of a few tens of nanometers.

Lattice images of polysaccharide crystals have generally been recorded perpendicular to the fiber axis of microfibrillar cellulose[50] or chitin[49,51] and, more rarely, parallel to the fiber axis.[48] To our knowledge, only one paper reports lattice imaging of lamellar V-amylose crystals.[52] However, the images do not allow the unambiguous recognition of 6-fold helices. Our HREM images thus appear to be the first that clearly show the organization of V-amylose helices in the (*a*, *b*) base plane of the crystal.

Fourier-space filtering procedures are generally used to reveal the molecular details in the noisy lattice images of biological and polymer materials.[53] The reflections in the Fourier transform of the original micrograph are selected using small circular masks and a filtered image is obtained by back-Fourier transforming the masked diffractogram. As demonstrated by Pradère et al.,[54] the artefacts associated with this method have to be carefully evaluated, in particular when the signal-to-noise ratio is very low. The real-space averaging procedure that we used in this work appeared to be a simple and efficient alternative to Fourier filtering. We compared real-space and Fourier-space methods on our lattice images. As both provided similar results, we decided to present here the one which is less commonly used. In order to consolidate our interpretation of the average image as a direct projection of a crystal containing 8-fold helices, our assumption about the PCTF and the atoms being black has to be verified. It is necessary to record more images using, if possible, different defocus values. One way to improve the yield in "good" images would be to work at liquid nitrogen or helium temperature, using highly stable specimen holders.

Up to now, the structure determination of the various types of V-amylose has led to some controversy. When surveying the unit cell parameters determined by various authors, one notices that the base plane dimensions vary depending on the crystal type. However, all types share a common repeat along the fiber axis, i.e., about 0.8 nm. Despite this common value, the authors have debated to know whether the amylose helices were 6-, 7-, or 8-fold depending on the complexing agent. The propositions to account for such a diversity are based on the similarity between helical amylose and α-, *β*-, and *γ*-cyclodextrins, composed of 6, 7, and 8 α-D-glucosyl units, respectively. These cyclic molecules have external diameters of 1.36, 1.47, and 1.64 nm, respectively.[55,56] Since the V_H structure is described as a close-packed arrangement of 6-fold helices that also have an external diameter of 1.36 nm,[11,13,15,57] the diameters of V_H amylose helices and α-cyclodextrins perfectly match.

The situation of $V_{n-butanol}$ crystals is more complex, and it is believed that the amylose helices are separated by intercalated *n*-butanol molecules to account for the larger unit cell parameters of the base plane.[21,29] Since the removal of the *n*-butanol molecules invariably leads to the V_H structure without modification of the crystal shape,[17,21,28,29] it seems logical that $V_{n-butanol}$ crystals also contain 6-fold amylose helices with an external diameter of 1.36 nm.

The case of $V_{isopropanol}$ crystals is not clear at the moment. On the one hand, one can conceive that they are made of 7-fold helices. Such larger helices have first been considered to account for the large unit cell of crystals of V-amylose complexed with *tert*-butyl alcohol,[55,58,59] which have the same unit cell as $V_{isopropanol}$. This unit cell can accommodate a number of 7-fold helices in close contact, with helices having an external diameter of 1.47 nm, i.e., that of *β*-cyclodextrin. On the other hand and in opposition to this argument, the fact that $V_{isopropanol}$ single crystals can readily be converted into the 6-fold V_H structure without loosing their perfection[22,26] and that they can be colored with iodine[33] is not in favor of the presence of 7-fold helices in these crystals. Thus, the $V_{isopropanol}$ structure could resemble that of $V_{n-butanol}$ and therefore could consist of 6-fold helices separated by isopropanol intercalates. In favor of this last assumption, the $V_{n-butanol}$ crystals can be converted into the $V_{isopropanol}$ crystalline type if they are soaked into cyclohexanone, and again they can do so without loosing their apparent

perfection.[29] Taken together, these observations leave open the existence of 7-fold amylose helices in V-amylose crystals.

The 8-fold amylose helices that are described in the present paper have an external diameter of 1.62 nm, which is very close to that of γ-cyclodextrins. The 8-fold helices markedly differ from those occurring in V_H, $V_{n-butanol}$, and $V_{isopropanol}$ crystals. Their helical structure appears to be quite stable as it was not possible to convert them into V_H by removing the complexing agent. In the same manner, iodine, which could permeate the 6-fold helices in the crystals of V_H, $V_{n-butanol}$, or $V_{isopropanol}$, could not do so in the case of $V_{\alpha-naphthol}$.[33] Thus, while the occurrence of the 7-fold helices in $V_{isopropanol}$ complexes is still questioned, we are quite convinced of the 8-fold structure in the case of $V_{\alpha-naphthol}$ crystals. It is clear that if the electron crystallography treatment that was applied to the $V_{\alpha-naphthol}$ crystals could be also performed for $V_{isopropanol}$ and the $V_{n-butanol}$ crystals, all ambiguities about the 7-fold helices would be lifted.

One may wonder why the $V_{\alpha-naphthol}$ crystals presented in this study have a crystallinity substantially better than those of the other V-amylose complexes despite crystallization procedures that are very similar. One of the reasons may be found in our use of synthetic amylose. Indeed, this amylose, which is perfectly linear, differs from the commercial fractions that were used earlier.[33] The amylose fractions extracted from starch are known to contain a certain degree of branching, a feature that is detrimental for the preparation of defect-free crystals. In addition to its linearity, the amylose we used has an average DP of 100. Assuming a rise per glucosyl monomer of about 0.1 nm, 8-fold helices formed with DP 100 amylose would have a length of roughly 10 nm. Consequently, there is no need for the amylose chains to fold back and forth to produce crystalline lamellae with a thickness of about 10 nm. Indeed, the chain-folding mechanism is easily observed with flexible synthetic polymers but is more difficult with semirigid polymers such as underivatized polysaccharides, for which the best lamellar crystals have systematically been obtained when the chains were short enough to avoid chain-folding.[60] Thus, even if in amylose, the possibility of chain flipping[23] could favor a tight folding of the chains, we think that chains of DP 100 have an optimal length to form folding-free and therefore defect-less crystals.

A salient result from this work is the collection of good sets of three-dimensional diffraction data on the $V_{\alpha-naphthol}$ crystals. Work is in progress to resolve the crystal structure by combining conformational and packing analyses together with a structure refinement based on electron and X-ray diffraction data. Lattice images will then be simulated from the resulting models using multislice calculation and compared to the experimental micrographs.

Acknowledgment. The authors thank K. Gessler for the gift of a sample of synthetic amylose and some preliminary contribution to this work. We also acknowledge P. Pattison for his help with the data acquisition at ESRF. M.B.C. received a fellowship from the Coordenação de Aperfeiçoamento de Pessoal de Nível Superior (CAPES) from Brazil.

Supporting Information Available. List of reflections observed in electron diffraction patterns recorded at room temperature on untilted and tilted single crystals. List of a selection of nonoverlapping *d*-spacings observed in synchrotron X-ray diffraction diagrams recorded on dry mats of $V_{\alpha-naphthol}$ crystals. This material is available free of charge via the Internet at http://pubs.acs.org.

References and Notes

(1) Katz, J. R. Z. *Phys. Chem.* **1930**, *A150*, 37−59.
(2) Wu, H. C. H.; Sarko, A. *Carbohydr. Res.* **1978**, *61*, 7−25.
(3) Wu, H. C. H.; Sarko, A. *Carbohydr. Res.* **1978**, *61*, 27−40.
(4) Imberty, A.; Buléon, A.; Vinh, T.; Pérez, S. *Starch/Staerke* **1991**, *43*, 375−384.
(5) Buléon, A.; Duprat, F.; Booy, F. P.; Chanzy, H. *Carbohydr. Polym.* **1984**, *4*, 161−173.
(6) Pfannemüller, B. *Int. J. Biol. Macromol.* **1987**, *9*, 105−108.
(7) Gidley, M. J.; Bulpin, P. V. *Carbohydr. Res.* **1987**, *161*, 291−300.
(8) Sarko, A.; Zugenmaier, P. In *Fiber Diffraction Methods*; French, A. D.; Gardner, K. H., Eds.; ACS Symposium Series 141; American Chemical Society: Washington, DC, 1980; pp 459−482.
(9) Tomasik, P.; Schilling, C. H. *Adv. Carbohydr. Chem. Biochem.* **1998**, *53*, 263−343.
(10) Tomasik, P.; Schilling, C. H. *Adv. Carbohydr. Chem. Biochem.* **1998**, *53*, 345−426.
(11) Zaslow, B.; Murphy, V. G.; French, A. D. *Biopolymers* **1974**, *13*, 779−790.
(12) Murphy, V. G.; Zaslow, B.; French, A. D. *Biopolymers* **1975**, *14*, 1487−1501.
(13) Rappenecker, G.; Zugenmaier, P. *Carbohydr. Res.* **1981**, *89*, 11−19.
(14) Bluhm, T. L.; Zugenmaier, P. *Carbohydr. Res.* **1981**, *89*, 1−10.
(15) Brisson, J.; Chanzy, H.; Winter, W. T. *Int. J. Biol. Macromol.* **1991**, *13*, 31−39.
(16) Bittiger, H.; Husemann, E. *Koll. Z. Z. Polym.* **1969**, *232*, 661−668.
(17) Manley, R. St. J. *J. Polym. Sci. Part A* **1964**, *2*, 4503−4515.
(18) Yamashita, Y.; Ryugo, J.; Monobe, K. *J. Electron Microsc.* **1973**, *22*, 19−26.
(19) Welland, E. L.; Donald, A. M. *Int. J. Biol. Macromol.* **1991**, *13*, 69−72.
(20) Whittam, M. A.; Orford, P. D.; Ring, S. G.; Clark, S. A.; Parker, M. L.; Cairns, P.; Miles, M. *Int. J. Biol. Macromol.* **1989**, *11*, 339−344.
(21) Booy, F. P.; Chanzy, H.; Sarko, A. *Biopolymers* **1979**, *18*, 2261−2266.
(22) Buléon, A.; Delage, M. M.; Brisson, J.; Chanzy, H. *Int. J. Biol. Macromol.* **1990**, *12*, 25−33.
(23) Jacob, J.; Gessler, K.; Hoffmann, D.; Sanbe, H.; Koizumi, K.; Smith, S. M.; Takaha, T.; Saenger, W. *Angew. Chem., Int. Ed.* **1998**, *37*, 606−608.
(24) Gessler, K. Uson, I.; Takaha, T.; Krauss, N.; Smith, S. M.; Okada, S.; Sheldrick, G. M.; Saenger, W. *Proc. Natl. Acad. Sci. U.S.A.* **1999**, *96*, 4246−4251.
(25) Nimz, O.; Gessler, K.; Uson, I.; Sheldrick, G. M.; Saenger, W. *Carbohydr. Res.* **2004**, *339*, 1427−1437.
(26) Yamashita, Y.; Hirai, N. *J. Polym. Sci. Part A-2* **1966**, *4*, 161−171.
(27) Nuessli, J.; Putaux, J. L.; Le Bail, P.; Buléon, A. *Int. J. Biol. Macromol.* **2000**, *33*, 227−234.
(28) Yamashita, Y. *J. Polym. Sci. Part A* **1965**, *3*, 3251−3260.
(29) Helbert, W.; Chanzy, H. *Int. J. Biol. Macromol.* **1994**, *16*, 207−213.
(30) Hulleman, S. H. D.; Helbert, W.; Chanzy, H. *Int. J. Biol. Macromol.* **1996**, *18*, 115−122.
(31) Yamashita, Y.; Monobe, K. *J. Polym. Sci. Part A-2* **1971**, *9*, 1471−1481.
(32) Winter, W. T.; Chanzy, H.; Putaux, J. L.; Helbert, W. *Polym. Prepr.* **1998**, *39*, 703.
(33) Helbert, W. Doctoral dissertation, Joseph Fourier University of Grenoble, France, 1994.
(34) Winter, W. T.; Sarko, A. *Biopolymers* **1974**, *13*, 1447−1460.
(35) Winter, W. T.; Sarko, A. *Biopolymers* **1974**, *13*, 1461−1482.
(36) Godet, M. C.; Tran, V.; Delage, M. M.; Buléon, A. *Int. J. Biol. Macromol.* **1993**, *15*, 11−16.
(37) Godet, M. C.; Buléon, A.; Tran, V.; Colonna, P. *Carbohydr. Polym.* **1993**, *21*, 91−95.
(38) Grubb, D. T. *J. Mater. Sci.* **1974**, *9*, 1715−1736.
(39) Saxton, W. O.; Pitt, T. J.; Horner, M. *Ultramicroscopy* **1979**, *4*, 343−353.
(40) Sonneveld, E. J.; Visser, J. W. *J. Appl. Crystallogr.* **1975**, *8*, 1−7.
(41) Nishiyama, Y.; Langan, P. Chanzy, H. *J. Am. Chem. Soc.* **2002**, *124*, 9074−9082.
(42) Sugiyama, J.; Otsuka, Y.; Murase, H.; Harada, H. *Holzforschung* **1986**, *40*, suppl. 31−36.

(43) Revol, J. F. *J. Mater. Sci. Lett.* **1985**, *4*, 1347−1349.
(44) Saxton, W. O.; Baumeister, W. *J. Microsc.* **1982**, *127* (pt2), 127−138.
(45) Erickson, H. P.; Klug, A. *Philos. Trans. R. Soc. London, Ser. B* **1971**, *261*, 105−118.
(46) Thon, F. In *Electron Microscopy in Materials Science*; Valdre, U., Ed.; Academic Press: London, 1971; pp 571−625.
(47) Sugiyama, J.; Harada, H.; Fujiyoshi, Y.; Uyeda, N. *Planta* **1985**, *166*, 161−168.
(48) Helbert, W.; Nishiyama, Y.; Okano, T.; Sugiyama, J. *J. Struct. Biol.* **1998**, *124*, 42−50.
(49) Saito, Y.; Okano, T.; Chanzy, H.; Sugiyama, J. *J. Struct. Biol*. **1995**, *114*, 218−228.
(50) Imai, T.; Putaux, J. L.; Sugiyama, J. *Polymer* **2003**, *44*, 1871−1879.
(51) Revol, J. F.; Gardner, K. H.; Chanzy, H. *Biopolymers* **1988**, *27*, 345−350.
(52) Miller, D.; Sugiyama, J.; Brisson, J.; Chanzy, H. In *Electron Crystallography of Organic Molecules*; Fryer, J. R., Dorset, D. L., Eds.; Kluwer Academic Publishers, 1990; pp 189−195.
(53) Stewart, M. *J. Electron Microsc. Tech.* **1988**, *9*, 301−324.
(54) Pradère, P.; Revol, J. F.; Nguyen, L.; St. John Manley, R. *Ultramicroscopy* **1988**, *25*, 69−80.
(55) Takeo, K.; Kuge, T. *Agric. Biol. Chem.* **1969**, *33*, 1174−1180.
(56) Takeo, K.; Kuge, T. *Agric. Biol. Chem*. **1970**, *34*, 568−574.
(57) Mikus, F. F.; Hixon, R. M.; Rundle, R. E. *J. Am. Chem Soc.* **1946**, *68*, 1115−1123.
(58) Bear, R. S. *J. Am Chem. Soc.* **1944**, *66*, 2122−2123.
(59) Zaslow, B. *Biopolymers* **1963**, *1*, 165−169.
(60) Buléon, A.; Chanzy, H.; Froment, P. *J. Polym. Sci. Polym. Phys. Ed.* **1982**, *20*, 1081−1088.

BM0611174